RESEARCH ARTICLE

Effectively improve the mechanical properties of carbon fabric/epoxy composites by oxidized carbon nitride

Song-Qing Zhu[1,2,3] | Jing-Jing Lu[1] | Meng-Xuan Fan[1,3] |
Yelizaveta Chernysh[4,5] | Ya-Jie Pan[1] | Rui-Qiong Dang[1] |
Ji-Peng Guan[1] | Li-Chao Yu[1] | Ben-Cai Lin[3] | Xiao-Jun Shen[1]

[1]Key Laboratory of Yarn Materials Forming and Composite Processing Technology of Zhejiang Province, Jiaxing University, Jiaxing, China

[2]Group of Mathematics Teaching and Research, Tonglu County Zhaixi Primary School, Tonglu, China

[3]School of Materials Science and Engineering, Changzhou University, Changzhou, China

[4]Department of Applied Ecology, Sumy State University, Sumy, Ukraine

[5]Faculty of Tropical AgriSciences, Czech University of Life Sciences Prague, Prague, Czech Republic

Correspondence
Xiao-Jun Shen, Key Laboratory of Yarn Materials Forming and Composite Processing Technology of Zhejiang Province, Jiaxing University, Jiaxing 314001, China.
Email: sxj908@163.com

Abstract

In this work, carbon nitride (C_3N_4) powder was oxidized by the Hummers oxidation method, and oxidized carbon nitride (O-C_3N_4) was obtained. Epoxy (EP) was modified with O-C_3N_4, and then carbon fiber fabric/epoxy (CF/EP) composites were prepared by hand-pasting molding. The O-C_3N_4 greatly improves the wettability of EP resin, enhances the interface properties of CF/EP composites, and makes the composites have better mechanical properties. The interlaminar shear strength (ILSS) is increased from 51.75 to 59.68 MPa, the tensile strength is increased from 564.54 to 635.39 MPa, the bending strength is increased from 809.64 to 938.81 MPa, and the impact strength is increased from 73.48 to 84.84 kJ/m^2. Meanwhile, the dynamic mechanical properties of composites are also significantly improved. The energy storage modulus is increased from 14.9 to 21.4 GPa, with an increase of 43.6%.

Highlights

- Developing carbon fiber composites is conducive to industrial applications.
- O-C_3N_4 effectively improves the mechanical properties of the composite.
- O-C_3N_4 has the advantages of simple synthesis, low costs, and light color.
- O-C_3N_4 is rich in oxygen-containing functional groups.

KEYWORDS
composites, mechanical properties, modification

1 | INTRODUCTION

Due to their low weight and high specific strength, carbon fiber-reinforced epoxy resin composites are utilized extensively in the aerospace, civil engineering, automotive, sporting goods, and other areas.[1–3] Interlaminar shear strength (ILSS) is typically a significant design consideration for CF/EP laminated composites. And interface acts as a bridge for bonding and load transfer between CF and EP, which has a critical impact on the final performance of CF/EP composites.[4–8] However, the poor interfacial compatibility of CF with EP results in lower mechanical strength, which seriously limits the further development and application of CF/EP composites.[9–14] To achieve high mechanical properties of CF/EP composites, it is necessary to improve the interface properties of CF/EP composites.

Nowadays, there are two main methods to improve the mechanical properties of fiber-reinforced polymer matrix composites. The first method is to modify fiber, including coupling agent treatment, surface grafting treatment, plasma treatment, and γ-ray treatment.[15–17] Modifying polymer matrix resins is another method.[18–21] The latter modification method is low-cost and convenient to operate.[22] Cha et al.[23] introduced melamine-functionalized carbon nanotubes (CNTs) and melamine-functionalized graphene nanosheets (GNPs) into the epoxy matrix to improve the ILSS of the CF/EP composites. The incorporation of 2 wt% melamine@CNTs and melamine@GNPs increased the ILSS of the CF/EP composites by 61% and 219%, respectively. Suresha et al.[24] introduced organo-modified montmorillonite nanolayers into EP to enhance the composites. The bending strength, ILSS, impact strength, and modulus of elasticity of the composites increased with the increase in the content of organo-modified montmorillonite nanolayers.

Even though these works have good results, they cannot be used in industrial production because of their complicated processing methods and expensive materials. In our previous work,[25] we found that the oxidation treatment can make C_3N_4 have oxygen-containing functional groups, which can react with epoxy resin so that the interfacial adhesion between $O-C_3N_4$ and epoxy can be improved. Moreover, $O-C_3N_4$ is simple to prepare and can be produced in large quantities for industrial applications. And $O-C_3N_4$ is much cheaper than nanofillers such as carbon nanotubes and graphene. To the best of our knowledge, there is no report on the effect of $O-C_3N_4$ on improving the mechanical properties of CF/EP composites.

The purpose of this study was to improve the mechanical properties of CF/EP composites. To achieve the aim, the following tasks were solved: C_3N_4 was oxidized by the Hummers method to obtain $O-C_3N_4$, and then epoxy was modified with $O-C_3N_4$ to prepare $O-C_3N_4$/CF/EP composites. The reinforcing effect of $O-C_3N_4$ on CF/EP composite was evaluated by ILSS, tensile strength, bending strength, and impact toughness. The microstructure of composites was also analyzed. The results showed that the introduction of $O-C_3N_4$ could enhance and improve the wettability of EP to CF, and thus enhance the mechanical properties of CF/EP composites.

2 | MATERIALS AND METHODS

2.1 | Materials

Sinopharm Chemical Reagent Co., Ltd. supplied potassium permanganate, sodium nitrate, concentrated sulfuric acid (98.0%), and hydrochloric acid (38.0%). Jiangsu Qiangsheng Functional Chemical Co., Ltd supplied hydrogen peroxide (30%). Epoxy resin (E-51) and curing agent (593) were purchased from Haining Hailong Chemical Co., Ltd. CF (T300 3 K, 0°/90° orthogonal weave) was obtained from Longxin Co., Ltd. The chemicals used in this study are all reagent grade and do not require further purification.

2.2 | Preparation of C_3N_4

The synthesized steps of C_3N_4 powders were strictly performed as follows: Firstly, 100 g melamine was transferred to a 200 mL crucible with cover. Then, it was calcined in a muffle furnace at 550°C for 4 h. Finally, the obtained yellow product was ground into powders by an agate mortar.

### 2.3 | Preparation of $O-C_3N_4$

$O-C_3N_4$ was prepared in a similar way to Hummers: a clean three-necked flask was placed in an ice bath at 0°C. Then concentrated sulfuric acid (31 mL), carbon nitride powder (4 g), sodium nitrate (0.7 g), and potassium permanganate (4 g) were slowly added to the flask successively. The above mixture was continuously stirred for 2 h. Then, the reaction was carried out at 35°C for 1 h. The temperature of the water bath was then raised to 98°C. To the aforesaid combination, 95 mL of deionized water was added and swirled for 15 min. The reaction was completed by adding 7 mL of hydrogen peroxide and 2 mL of hydrochloric acid. By washing the combination in deionized water until the pH reached 7, the $O-C_3N_4$ was produced, and the color was milky white. Then the $O-C_3N_4$ was ultrasonically treated for 4 h. The well-dispersed mixture of $O-C_3N_4$ was finally obtained.

2.4 | Preparation of $O-C_3N_4$/CF/EP composites

The $O-C_3N_4$ with different Phr relative to the epoxy resin and curing agent system was evenly dispersed in the epoxy matrix. And then the absolute ethanol in the mixture was removed by heating it in a water bath pot at 78°C. Finally, the EP containing different Phr of $O-C_3N_4$ was obtained.

The 12 layers of CF were dried at 80°C for 2 h to fully remove moisture. Then the curing agent was added to the epoxy resin containing different Phr of $O-C_3N_4$ and stirred thoroughly. Finally, the prepared epoxy

FIGURE 1 Schematic of preparation of O-C₃N₄/CF/EP composites.
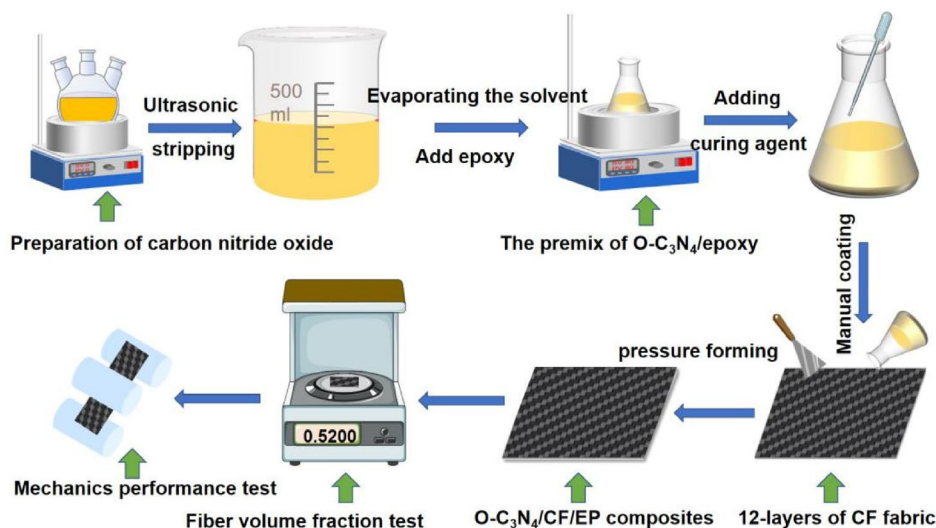
system mixture was evenly coated on 12 layers of CF by hand-paste molding technology. At room temperature, the O-C_3N_4/CF/EP composites were obtained by pressing and curing under the pressure of 5 MPa for 24 h with a plate vulcanizing machine. The manufacturing process of O-C_3N_4/CF/EP composites is shown in Figure 1.

2.5 | Characterization

The surface functional groups of C_3N_4 were investigated using Flourier transform infrared spectroscopy before and after oxidation. (FTIR, VERTEX 70, Germany). The crystal structure of C_3N_4 before and after oxidation was studied using X-ray diffraction (XRD, D8 ADVANCE, Germany). SEM was used to examine the microscopic morphology of C_3N_4 before and after oxidation, as well as the cross-sectional morphology of composites. (SEM, Thermo Scientific Apreo 2, Japan). Dynamic contact angle meter tests assessed CF and EP wettability. (DSA30, Germany).

The ILSS characteristics of the composites were measured using the interlaminar shear test standard. (ASTMD2344). Which were tested at a rate of 1 mm/min speed by using the Universal Mechanical Testing Machine (Shimadzu-AG-X plus, Japan). The tensile and bending properties of the composites were tested using the Universal Mechanical Testing Machine by the GB/T 16421–1996 and GB/T 1449–2005 standards. (Shimadzu-AG-X plus, Japan). The impact strength of the composites was measured using a pendulum impact testing machine by the GB/T 1451–2005 standard. (PTM2300, China). A dynamic thermomechanical analyzer (DMA Q850, USA) was used to evaluate the dynamic thermal-

mechanical behavior at a vibration frequency of 1 Hz and a temperature range of 35–130°C with a heating rate of 2°C/min. The three-point bending mode was adopted, and the sample dimensions were 30 mm × 6 mm × 2 mm.

3 | RESULTS AND DISCUSSION

3.1 | Characterization of O-C_3N_4

Through the use of scanning electron microscopy (SEM), the surface morphologies of C_3N_4 and C_3N_4 were observed. Figure 2A depicts the SEM of C_3N_4, which is primarily a 20–40 μm layered layering structure. In addition, O-C_3N_4 has the flake structure depicted in Figure 2B. According to the findings, the modified Hummers approach has the potential to successfully convert the layered stacking structure of C_3N_4 into a flaky structure.

Figure 3 displays the XRD patterns of C_3N_4 and O-C_3N_4. It can be observed that the peaks of C_3N_4 and O-C_3N_4 are quite the same, which suggests that the crystal structure of C_3N_4 and O-C_3N_4 are similar. The diffraction of the aromatic system's inter-planar stacking peak (002) after oxidation changes from 27.57° to a higher Angle (27.87°).[26] The corresponding crystal plane spacing of C_3N_4 and O-C_3N_4 can be computed as 0.324 nm and 0.320 nm, respectively, using the Bragg equation. This suggests that the O-C_3N_4 nanosheets that were produced have tighter stacking. The corridor distances between the basic sheets in the nanosheets are reduced as a result of the oxidized layers being flattened by the π-π stacking and hydrogen bond interactions, which results in denser packing.[27]
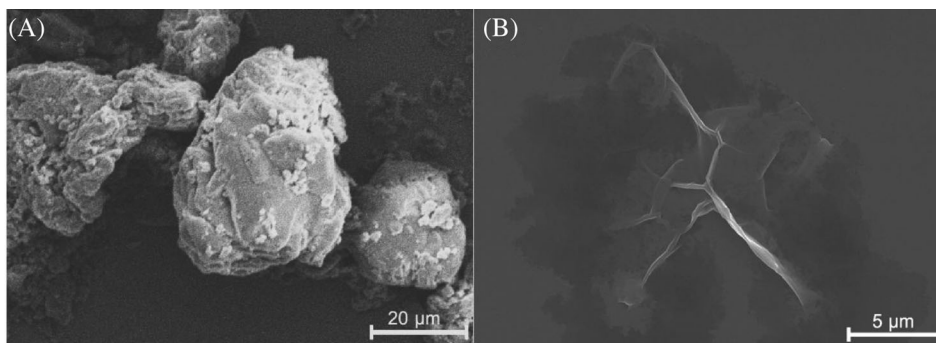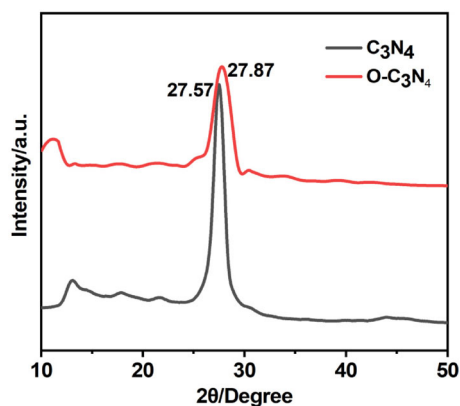
FIGURE 2 SEM images of (A) C_3N_4; (B) O-C_3N_4.

FIGURE 3 XRD patterns of C_3N_4 and O-C_3N_4.

TABLE 1 Density and CF volume fraction of O-C_3N_4/CF/EP composites.

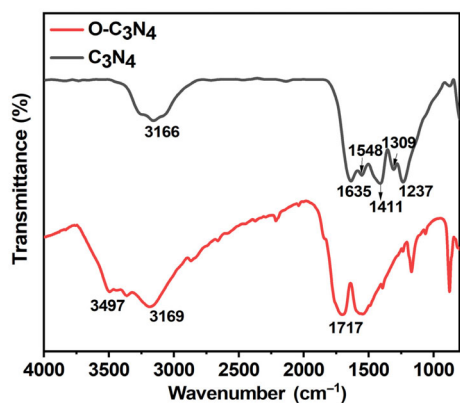| Composites	Fiber volume fraction (%)	Composites density (g/cm^3)
CF/EP	60.94 ± 0.16	1.44
0.1 phr O-C_3N_4/CF/EP	57.55 ± 0.35	1.43
0.3 phr O-C_3N_4/CF/EP	57.90 ± 0.44	1.44
0.5 phr O-C_3N_4/CF/EP	60.02 ± 0.67	1.45
0.7 phr O-C_3N_4/CF/EP	60.66 ± 0.40	1.49
1.0 phr O-C_3N_4/CF/EP	58.73 ± 0.49	1.42

FIGURE 4 FTIR of C_3N_4 and O-C_3N_4.

Figure 4 displays the FT-IR spectra of both C_3N_4 and O-C_3N_4, respectively. For the C_3N_4, the stretching vibration of C-NH$_2$ and the bending vibration of the s-triazine units are responsible for the characteristic peaks 810 cm^{-1} to 890 cm^{-1}.[28] And the peaks at 1237, 1309, 1411, 1548, and 1635 cm^{-1} may be attributed to the stretching vibration of C—N and C═N in the CN heterocyclic.[29] Furthermore, the absorption peak at 3166 cm^{-1} is the stretching vibration of NH$_2$.[30] For the O-C_3N_4, the obvious difference is that the O-C_3N_4 has absorption peaks

at 1717 cm^{-1} and 3497 cm^{-1}. The stretching vibration of C═O is responsible for the absorption peak that occurs at 1717 cm^{-1}, while the stretching vibration of —OH is responsible for the absorption peak that occurs at 3497 cm^{-1}.[27] The findings imply that the surface of O-C_3N_4 nanosheets contains oxygen-containing functional groups.

3.2 | Density and CF volume fraction of composites

The volume fraction of CF in the O-C_3N_4/CF/EP composites and the density of the composites were obtained by weighing and calculation. The results are shown in Table 1. It is clear to see that the volume fraction of CF in the composite material is maintained in the range of 57%–61%. And, the density of the composites maintained about 1.44 g/cm^3, which suggests that the addition of O-C_3N_4 will not greatly alter the density of the original composites.

3.3 | Dynamic contact angle analysis

To investigate the influence of O-C_3N_4 on the wettability of CF. The contact angles were measured when 0.5 Phr

O-C$_3$N$_4$ modified epoxy and pure epoxy were dropped onto the CF surface for 5 s and 10s. As shown in Figure 5, the contact angles between O-C$_3$N$_4$/EP and CF at 5 s (90°) and 10s (83°) (Figure 5A,B) were smaller than those between pure epoxy and CF at 5 s (130°) and 10s (100°) (Figure 5C,D), respectively. The results indicate that the EP with O-C$_3$N$_4$ has better wettability to CF. Therefore, O-C$_3$N$_4$ plays a significant role in improving the interface between CF and EP.[31]
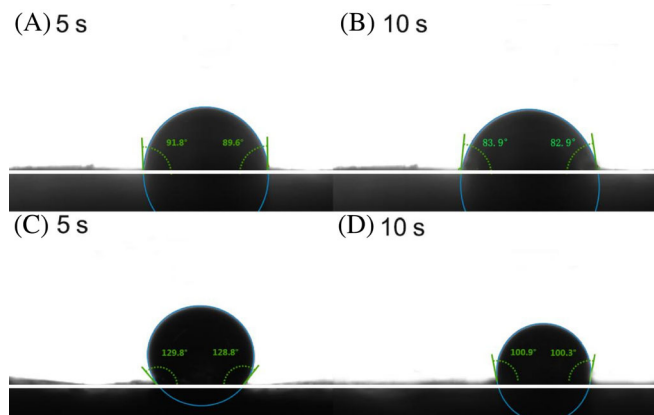

FIGURE 5 Contact angle photos of (A, B) 0.5 phr O-C$_3$N$_4$/EP and (C, D) pure epoxy drop onto the CF surface for 5 s and 10 s.

3.4 | Static mechanical properties of O-C$_3$N$_4$/CF/EP composites

Composite materials with good interfacial properties often exhibit good mechanical properties.[32–34] In this work, a three-point bending test was used to evaluate the ILSS. As illustrated in Figure 6A, the composite ILSS is 51.75 MPa without the addition of O-C$_3$N$_4$. When the O-C$_3$N$_4$ is introduced, the ILSS of composites increases with the increased addition of O-C$_3$N$_4$ and reaches the maximum (59.68 MPa) when the O-C$_3$N$_4$ content is 0.5 Phr. The increasing rate is 15.3%, compared with the CF/EP composite. The results show that the composites' interface is significantly improved after the introduction of O-C$_3$N$_4$, which can be attributed to the improved wettability of the EP modified by O-C$_3$N$_4$ to the CF.[31] Another important reason is that some O-C$_3$N$_4$ nanosheets are deposited on the CF surface by π–π interaction (Figure 6D). These O-C$_3$N$_4$ nanosheets are rich in oxygen-containing functional groups that can react with epoxy groups, so they can be tightly bound to epoxy resin, improving the interface between the two.

However, when the O-C$_3$N$_4$ component exceeds 0.5 Phr, the ILSS performance of the composites decreases, mainly because the excess O-C$_3$N$_4$ is not easily dispersed in the EP matrix. The aggregation of O-C$_3$N$_4$ will affect the infiltration of the matrix to the fiber and also cause
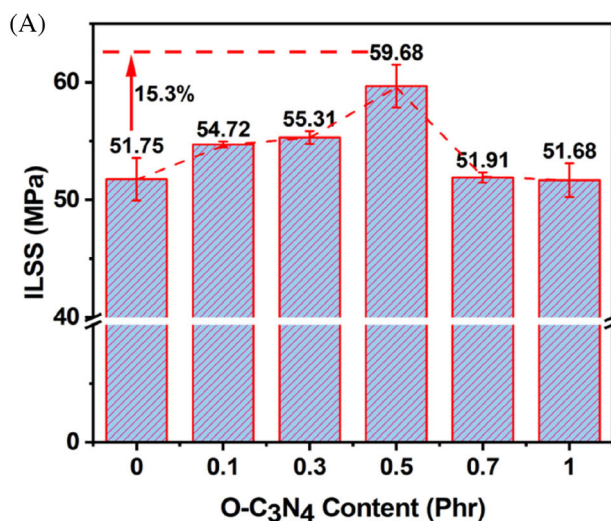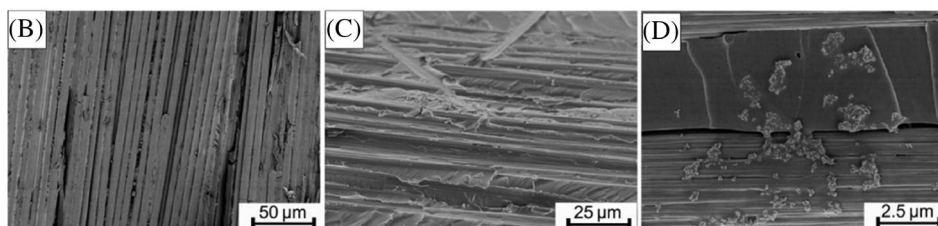

FIGURE 6 (A) ILSS properties of O-C$_3$N$_4$/CF/EP composites, and the SEM images of the peeling surface of (B) CF/EP; (C) 0.5 Phr O-C$_3$N$_4$/CF/EP; and (D) 1 Phr O-C$_3$N$_4$/CF/EP.

stress concentration.[35] Therefore, the ILSS of the composite decreases when more than 0.5 Phr $O-C_3N_4$ is used.

At the same time, the crack surface morphology of interlaminar shear splines was further explored. Figure 6B depicts the crack surface morphology of CF/EP composites. Due to the interface performance between CF and EP being poor, the composites will cause interfacial debonding when damaged by external forces. Therefore, the CF surface is smooth, and there is a gap between CF and EP.[36] However, the interface performance between CF and EP is enhanced after the introduction of $O-C_3N_4$. Figure 6C shows the crack surface morphology of 0.5 Phr $O-C_3N_4$/CF/EP composites. As can be seen, the EP is attached to the CF surface, so the interface between CF and EP has good adhesion. Therefore, the mechanical properties can be improved. However, when $O-C_3N_4$ content exceeds 0.5 Phr, it will reduce the dispersion of $O-C_3N_4$ and cause aggregation. Figure 6D shows the crack surface morphology of 1.0 Phr $O-C_3N_4$/CF/EP composites, and the aggregation phenomenon of $O-C_3N_4$ can be seen. These $O-C_3N_4$ aggregates are equivalent to introducing defects, forming stress concentration, and leading to mechanical property degradation.[37]

The findings of a tensile test that was conducted to investigate the impact that $O-C_3N_4$ has on the tensile strength of the composite are presented in Figure 7A. At an $O-C_3N_4$ content of 0.5 Phr, the tensile strength of the $O-C_3N_4$/CF/EP composite reaches a maximum value of 635.39 MPa, which is 12.6% higher than that of the pure CF/EP composite (564.54 MPa). This is mainly attributed to the strengthening effect of $O-C_3N_4$ on the epoxy matrix. The hydroxyl and carboxyl groups in $O-C_3N_4$ can chemically bond with epoxy groups, which improves the interface adhesion and enhances the mechanical properties.[38] As the EP infiltrates into CF in the process of hand-paste molding, some $O-C_3N_4$ is attached to the CF surface through π-π action, which is equivalent to playing the role of the bridge that connects CF and EP. If the composite is damaged by external forces, the stress can effectively transfer the load to the CF, and more force is required to break the bond between the CF and the EP.[39] Therefore, the addition of $O-C_3N_4$ can effectively improve the tensile strength of $O-C_3N_4$/CF/EP composites. However, the tensile strength of the composites decreases when the $O-C_3N_4$ content is more than 0.5 Phr because the excessive $O-C_3N_4$ will affect the infiltration of EP into the CF. And excessive $O-C_3N_4$ will produce an aggregation phenomenon, resulting in stress concentration, which is equivalent to introducing defects to the composites.

The tensile properties can be better explained by the microstructure of SEM. As can be seen from Figure 7B, the CF was pulled out without the addition of $O-C_3N_4$. The fracture length of the CF was varied, and the surface of the CF was smooth without epoxy adhesion. However, in Figure 7C, the CF is not easy to be pulled out after modification of $O-C_3N_4$, the CF breaks in a relatively neat manner, and the CF is bonded with EP.
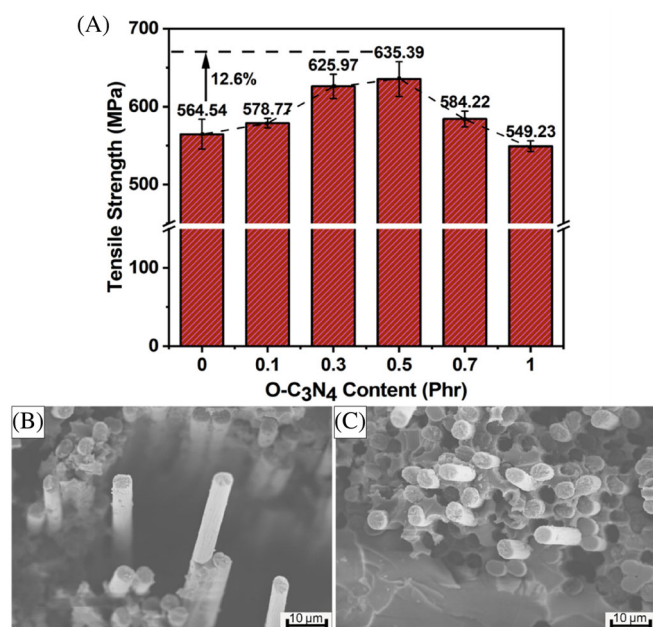

FIGURE 7 (A) Tensile properties of $O-C_3N_4$/CF/EP composites and the SEM images of a tensile section of (B) CF/EP; and (C) 0.5 Phr $O-C_3N_4$/CF/EP.
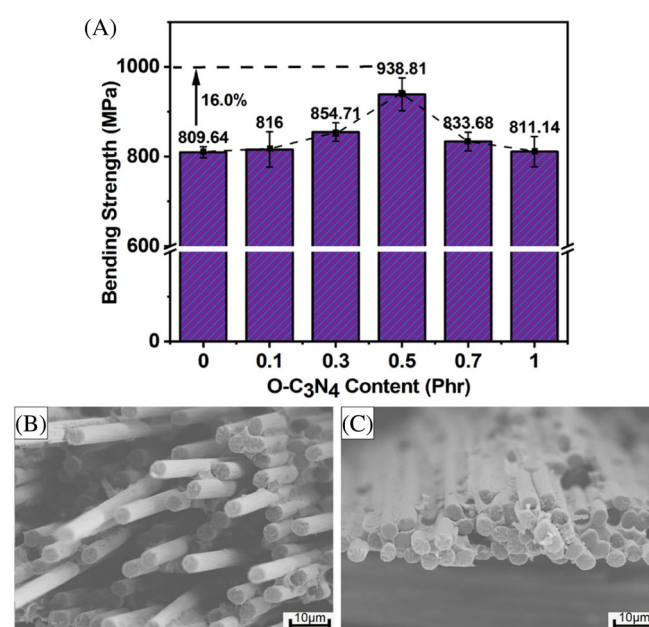

FIGURE 8 (A) Bending properties of $O-C_3N_4$/CF/EP composites and the SEM images of bending section of (B) CF/EP; (C) 0.5 Phr $O-C_3N_4$/CF/EP.

The effect of O-C$_3$N$_4$ on the bending characteristics of the composites was studied by using the bending properties test, the results are shown in Figure 8A. When the content of O-C$_3$N$_4$ is 0.5 Phr, the bending strength of O-C$_3$N$_4$/CF/EP composites can reach 938.81 MPa, which is 16.0% higher than that of pure CF/EP composites (809.64 MPa). This can be interpreted as the introduction of O-C$_3$N$_4$ to improve the interface adhesion between CF and EP, so the matrix can effectively transfer stress to CF. CF has the characteristics of high modulus, and the ability to withstand stress is stronger than epoxy resin matrix[40] so the bending properties of O-C$_3$N$_4$/CF/EP composites are improved. Similarly, the bending properties of the composites also decrease when the O-C$_3$N$_4$ content exceeds 0.5 Phr, which is mainly attributed to the

aggregation phenomenon caused by excessive O-C$_3$N$_4$ content, leading to stress concentration.

The enhanced bending properties can be better explained by the microstructure of SEM. As is evident from Figure 8B, when the composites were fractured under pressure perpendicular to the carbon fiber cloth without the addition of O-C$_3$N$_4$, the length of fracture of the CF was different, and the surface of the fiber was very smooth without epoxy adhesion. However, after modification of O-C$_3$N$_4$, as is evident (Figure 8C) that the CF fracture surface is very neat. The CF is firmly bonded with the EP, and the CF surface is adhered to the EP.

Here, impact performance is also discussed as an important index of the mechanical properties of composites. As can be seen from Figure 9A, the impact strength of O-C$_3$N$_4$/CF/EP composites can reach 84.84 kJ/m^2 when the O-C$_3$N$_4$ components are 0.5 Phr, which is 15.5% higher than pure composite (73.48KJ/m^2). Basically, this is because the addition of O-C$_3$N$_4$ strengthens the epoxy matrix, which acts as a reinforcing rod in the epoxy matrix. When the composite is damaged by external force, O-C$_3$N$_4$ can assume and transfer more stress, and change the path of the cracks, producing more microcracks during crack propagation. This complex crack propagation process can significantly improve the impact performance by consuming more energy.[41,42]

The enhanced impact properties can be better explained by the microstructure of SEM. In Figure 9B, as is evident that when without the addition of O-C$_3$N$_4$, the CF, and EP were completely debonded from the radial perspective, leaving smooth traces of CF pulled out on the epoxy surface. From the weft upwards, the CF is punctured very neatly, and the fiber surface is very smooth without epoxy adhesion. However, after modification of O-C$_3$N$_4$, as is evident (Figure 9C) that the CF and the EP were still attached from the perspective of the epoxy layer, and the epoxy wrapped the broken fiber. From the fiber layer, the length of the broken fibers is different, and the fibers are tightly bonded with the epoxy.
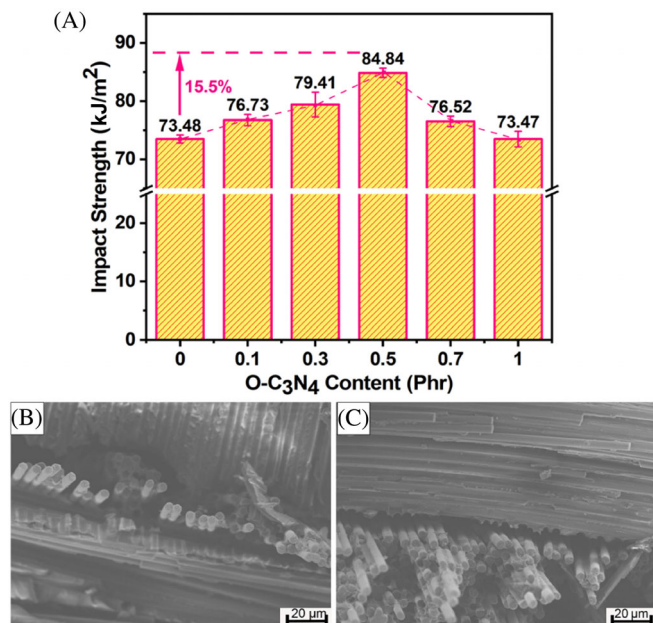

FIGURE 9 (A) impact properties of O-C$_3$N$_4$/CF/EP composites, and the SEM images of impact section of (B) CF/EP; (C) 0.5 Phr O-C$_3$N$_4$/CF/EP.
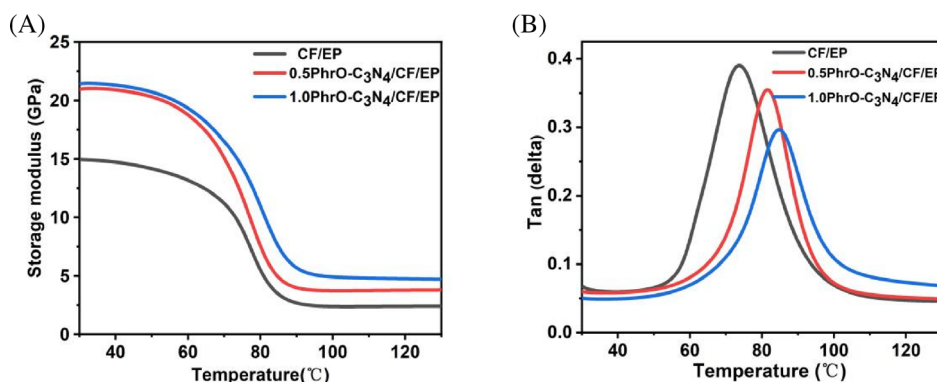

FIGURE 10 (A) Storage modulus and (B) tan δ curves for CF/EP composites and the O-C$_3$N$_4$/CF/EP composites.

3.5 | Dynamic mechanical properties of composites

Additionally, the influence of various O-C$_3$N$_{4v}$ contents on the dynamic mechanical properties of CF/EP composites was investigated. The dynamic mechanical properties of CF composites were examined by DMA. Figure 10 illustrates how the temperature affects the storage modulus (E') and loss factor (tan δ) for CF/EP composites and O-C$_3$N$_4$/CF/EP composites. Compared with CF/EP composites, O-C$_3$N$_4$/CF/EP composites have a higher E′ (Figure 10A). And with the higher content of O-C$_3$N$_4$, the E' of the O-C$_3$N$_4$/CF/EP composite becomes greater. When the content of O-C$_3$N$_4$ is 1.0 Phr, E' can reach 21.4 GPa, which is 43.6% higher than pure CF/EP composites (14.9 GPa). The result shows that the introduction of O-C$_3$N$_4$ can effectively enhance the stiffness of the composite. This is because the hydroxyl and carboxyl groups in O-C$_3$N$_4$ react with the hydroxyl and epoxy groups in the epoxy resin, which can bind O-C$_3$N$_4$ more tightly with the EP matrix and improve the strength of the epoxy itself. Moreover, the O-C$_3$N$_4$ can improve the wettability of EP to CF, modify the interface between CF and EP, and make the composites have better integrity.[43] Thus, the stiffness of the O-C$_3$N$_4$/CF/EP composite is increased.

Furthermore, the tan δ curves illustrate that O-C$_3$N$_4$/CF/EP composites have higher Tg and lower tan δ compared with pure CF/EP composites (Figure 10B). And it can be found that with the increase of O-C$_3$N$_4$ content, the increase of Tg is more obvious. When the content of O-C$_3$N$_4$ is 1.0 Phr, the Tg of O-C$_3$N$_4$/CF/EP composites can reach 85.0°C, which is 11.1°C higher than pure CF/EP composites (73.9°C). This phenomenon can be attributed to the introduction of O-C$_3$N$_4$ hindering the migration of polymer chains.[44] Another reason is that O-C$_3$N$_4$ improves the wettability between the EP and CF, which increases the interfacial compatibility, thereby enhancing the crosslink density of the interphase.[32] It can be proved that the addition of O-C$_3$N$_4$ can improve the thermal stability of O-C$_3$N$_4$/CF/EP composites.

4 | CONCLUSIONS

In this work, the O-C$_3$N$_4$/CF/EP composites were fabricated by hand-pasting molding. The O-C$_3$N$_4$ significantly improves the wettability of epoxy to CF, enhancing the interfacial properties of CF composites. The significantly improved interfacial properties guarantee excellent mechanical properties of CF composites. The ILSS of CF composites increased from 51.75 MPa to 59.68 MPa. The tensile strength and flexural strength increased from 564.54 MPa to 635.39 MPa and 809.64 MPa to 938.81 MPa, respectively. And the impact strength increased from 73.48KJ/m^2 to 84.84KJ/m^2. In addition, the dynamic mechanical properties of CF laminates were also significantly improved. After the introduction of O-C$_3$N$_4$, the E′ of O-C$_3$N$_4$/CF/EP composites can reach 21.4 GPa, which is 43.6% higher than pure CF/EP composites (14.9GPa). The Tg of the composites was also increased from 73.9°C to 85.0°C. Therefore, O-C$_3$N$_4$/CF/EP composites can be produced in large quantities for industrial applications due to their simple preparation and excellent mechanical properties.

DATA AVAILABILITY STATEMENT
The data that support the findings of this study are available from the corresponding author upon reasonable request.

ORCID
Xiao-Jun Shen https://orcid.org/0000-0003-1951-0927

REFERENCES

1. Chandrasekaran VCS, Advani SG, Santare MH. Influence of resin properties on interlaminar shear strength of glass/epoxy/MWNT hybrid composites. *Compos Part A: Appl Sci Manuf.* 2011;42(8):1007-1016. doi:10.1016/j.compositesa.2011.04.004

2. Liu Y, Yang JP, Xiao HM, et al. Role of matrix modification on interlaminar shear strength of glass fibre/epoxy composites. *Compos B: Eng.* 2012;43(1):95-98. doi:10.1016/j.compositesb.2011.04.037

3. Wang FZ, Drzal LT, Qin Y, Huang ZX. Size effect of graphene nanoplatelets on the morphology and mechanical behavior of glass fiber/epoxy composites. *J Mater Sci.* 2016;51(7):3337-3348. doi:10.1007/s10853-015-9649-x

4. Bedi HS, Tiwari M, Agnihotri PK. Quantitative determination of size and properties of interphases in carbon nanotube-based multiscale composites. *Carbon.* 2018;132:181-190. doi:10.1016/j.carbon.2018.02.059

5. Sun HG, Yang XB, Zhang YQ, et al. Segregation-induced in situ hydrophilic modification of poly (vinylidene fluoride) ultrafiltration membranes via sticky poly (ethylene glycol) blending. *J Membr Sci.* 2018;563:22-30. doi:10.1016/j.memsci.2018.05.046

6. Gu HB, Zhang HY, Lin J, et al. Large negative giant magneto-resistance at room temperature and electrical transport in cobalt ferrite-polyaniline nanocomposites. *Polymer.* 2018;143: 324-330. doi:10.1016/j.polymer.2018.04.008

7. Gu JW, Li Y, Liang CB, et al. Synchronously improved dielectric and mechanical properties of wave-transparent laminated

composites combined with outstanding thermal stability by incorporating iysozyme/POSS functionalized PBO fibers. *J Mater Chem*. 2018;6(28):7652-7660. doi:10.1039/c8tc02391c

8. Guan XY, Zheng GQ, Dai K, et al. Carbon Nanotubes-Adsorbed Electrospun PA66 Nanofiber Bundles with Improved Conductivity and Robust Flexibility. *ACS Appl Mater Interfaces*. 2016;8(22):14150-14159. doi:10.1021/acsami.6b02888

9. Yang XB, Wang ZX, Shao L. Construction of oil-unidirectional membrane for integrated oil collection with lossless transportation and oil-in-water emulsion purification. *J Membr Sci*. 2018;549:67-74. doi:10.1016/j.memsci.2017.11.071

10. Du XS, Liu HY, Xu F, Zeng Y, Mai YM. Flame synthesis of carbon nanotubes onto carbon fiber woven fabric and improvement of interlaminar toughness of composite laminates. *Compos Sci Technol*. 2014;101:159-166. doi:10.1016/j.compscitech.2014.07.011

11. Du XS, Zhou HLZ, Sun WF, et al. Graphene/epoxy interleaves for delamination toughening and monitoring of crack damage in carbon fibre/epoxy composite laminates. *Compos Sci Technol*. 2017;140:123-133. doi:10.1016/j.compscitech.2016.12.028

12. Guo J, Song HX, Liu H, et al. Polypyrrole-interface-functionalized nano-magnetite epoxy nanocomposites as electromagnetic wave absorbers with enhanced flame retardancy. *J Mater Chem C*. 2017;5(22):5334-5344. doi:10.1039/c7tc01502j

13. Guo YQ, Xu GJ, Yang XT, et al. Significantly enhanced and precisely modeled thermal conductivity in polyimide nanocomposites with chemically modified graphene via in situ polymerization and electrospinning-hot press technology. *J Mater Chem C*. 2018;6(12):3004-3015. doi:10.1039/c8tc00452h

14. Xie PT, Li HY, He B, et al. Bio-gel derived nickel/carbon nanocomposites with enhanced microwave absorption. *J Mater Chem C*. 2018;6(32):8812-8822. doi:10.1039/c8tc02127a

15. Yaman N, Senol MF. Shear Behavior of Glass Fabric/Epoxy Resin Composite Prepared by Surface Treatments. *Aatcc Rev*. 2012;12(2):73-79.

16. Carvelli V, Gramellini G, Lomov SV, Bogdanovich AE, Mungalov DD, Verpoest I. Fatigue behavior of non-crimp 3D orthogonal weave and multi-layer plain weave E-glass reinforced composites. *Compos Sci Technol*. 2010;70(14):2068-2076. doi:10.1016/j.compscitech.2010.08.002

17. Ma D, Li Y, Sun T, Fan L, Wang P, Xiao J. Tensile properties of z-pins reinforced laminates. *Polym Polym Compos*. 2011;19(4–5):251. doi:10.1177/0967391111019004-501

18. Zaheer U, Zulfiqar U, Khurram AA, Subhani T. Improving the performance of conventional glass fiber epoxy matrix composites by incorporating nanodiamonds. *Compos Interface*. 2018;25(11):1005-1018. doi:10.1080/09276440.2018.1454145

19. Cho J, Daniel IM. Reinforcement of carbon/epoxy composites with multi-wall carbon nanotubes and dispersion enhancing block copolymers. *Scr Mater*. 2008;58(7):533-536. doi:10.1016/j.scriptamat.2007.11.011

20. Quaresimin M, Salviato M, Zappalorto M. Fracture and interlaminar properties of clay-modified epoxies and their glass reinforced laminates. *Eng Fract Mech*. 2012;81:80-93. doi:10.1016/j.engfracmech.2011.10.004

21. Jia JJ, Du XS, Chen C, Sun XY, Mai YW, Kim JK. 3D network graphene interlayer for excellent interlaminar toughness and strength in fiber reinforced composites. *Carbon*. 2015;95:978-986. doi:10.1016/j.carbon.2015.09.001

22. Cha JM, Kim JH, Ryu SW, Hong SH. Strengthening effect of melamine functionalized low-dimension carbon at fiber reinforced polymer composites and their interlaminar shear behavior. *Compos B: Eng*. 2019;173:1-8. doi:10.1016/j.compositesb.2019.106976

23. Han X, Zhao Y, Sun JM, Li Y, Zhang JD, Hao Y. Effect of graphene oxide addition on the interlaminar shear property of carbon fiber-reinforced epoxy composites. *N Carbon Mater*. 2017;32(1):48-55. doi:10.1016/S1872-5805(17)60107-0

24. Suresha B, Saini MS. Influence of organo-modified montmorillonite nanolayers on static mechanical and dynamic mechanical behavior of carbon/epoxy composites. *J Compos Mater*. 2015;50(25):3589-3601. doi:10.1177/0021998315622984

25. Zhu SQ, Fan MX, Zhao SH, et al. Epoxy resin composites reinforced with sheet stripping oxidized carbon nitride. *J Mater Sci*. 2022;57(43):20187-20196. doi:10.1007/s10853-022-07899-x

26. Li HJ, Sun BW, Sui L, Qian DJ, Chen M. Preparation of water-dispersible porous g-C_3N_4 with improved photocatalytic activity by chemical oxidation. *Phys Chem Chem Phys*. 2015;17(5):3309-3315. doi:10.1039/c4cp05020g

27. Feng J, Chen TT, Liu SN, et al. Improvement of g-C_3N_4 photocatalytic properties using the Hummers method. *J Colloid Interface Sci*. 2016;479:1-6. doi:10.1016/j.jcis.2016.06.040

28. Sh L, Chang K, Zhang HB, et al. Drastic enhancement of photocatalytic activities over phosphoric acid protonated porous g-C_3N_4 nanosheets under visible light. *Small*. 2016;12(32):4431-4439. doi:10.1002/smll.201601668

29. Li K, Gao SM, Wang QY, Xu H, Lu J. In-Situ-Reduced Synthesis of Ti^{3+} Self-Doped TiO_2/g-C_3N_4 Heterojunctions with High Photocatalytic Performance under LED Light Irradiation. *ACS Appl Mater Interfaces*. 2015;7(17):9023-9030. doi:10.1021/am508505n

30. Shen LY, Xing ZP, Zou JL. Black TiO(2) nanobelts/g-C(3)N (4) nanosheets laminated heterojunctions with efficient visible-light-driven photocatalytic performance. *Report*. 2017;7:41978. doi:10.1038/srep41978

31. Chen X, Xu HB, Liu D, Yan C, Zhu YD. A facile one-pot fabrication of polyphosphazene microsphere/carbon fiber hybrid reinforcement and its effect on the interfacial adhesion of epoxy composites. *Appl Surf Sci*. 2017;410:530-539. doi:10.1016/j.apsusc.2017.03.104

32. Song B, Wang TT, Wang L, et al. Interfacially reinforced carbon fiber/epoxy composite laminates via in-situ synthesized graphitic carbon nitride (g-C_3N_4). *Compos B: Eng*. 2019;158:259-268. doi:10.1016/j.compositesb.2018.09.081

33. Lu JJ, Shi YC, Dang RQ, et al. Modified mechanical properties of carbon fiber/epoxy composite by silicone polymer. *Polym Compos*. 2023;44(9):6039-6048. doi:10.1002/pc.27545

34. Lu JJ, Dang RQ, Zhang W, et al. Investigation on preparation and mechanical properties of carbon fiber fabric/hollow glass beads/epoxy resin sandwich composite laminates. *Polym Compos*. 2023;44(1):356-364. doi:10.1002/pc.27101

35. Pothan LA, Potschke P, Habler R, Thomas S. The static and dynamic mechanical properties of banana and glass fiber woven fabric-reinforced polyester composite. *J Compos Mater*. 2005;39(11):1007-1025. doi:10.1177/0021998305048737

36. Song B, Wang TT, Sun HG, et al. Graphitic carbon nitride (g-C_3N_4) interfacially strengthened carbon fiber epoxy composites. *Compos Sci Technol*. 2018;167:515-521. doi:10.1016/j.compscitech.2018.08.031

37. Chandrasekaran S, Sato N, Toelle F, Mulhaupt R, Fiedler B, Schulte K. Fracture toughness and failure mechanism of graphene based epoxy composites. *Compos Sci Technol.* 2014;97: 90-99. doi:10.1016/j.compscitech.2014.03.014

38. Wang Y, Raman Pillai SK, Che J, Chan-Park MB. High interlaminar shear strength enhancement of carbon fiber/epoxy composite through fiber-and matrix-anchored carbon nanotube networks. *ACS Appl Mater Interfaces.* 2017;9(10):8960-8966. doi:10.1021/acsami.6b13197

39. Xiong C, Li T, Zhao T, Dang A, Li H, Ji X. Reduced graphene oxide-carbon nanotube grown on carbon fiber as binder-free electrode for flexible high-performance fiber supercapacitors. *Compos B: Eng.* 2017;116:7-15. doi:10.1016/j.compositesb.2017.02.028

40. Nie HJ, Xu Z, Tang BL. The effect of graphene oxide modified short carbon fiber on the interlaminar shear strength of carbon fiber fabric/epoxy composites. *J Mater Sci.* 2021;56(1):488-496. doi:10.1007/s10853-020-05286-y

41. Subha S, Saira VNV, Pal Y. Effect of Zr/Gnp hybrid filler on thermal and ablation properties of carbon-epoxy composites. *Polym Compos.* 2020;42(2):642-651. doi:10.1002/pc.25854

42. Wong DWY, Lin L, McGrail PT, Peijs T, Hogg PJ. Improved fracture toughness of carbon fibre/epoxy composite laminates using dissolvable thermoplastic fibres. *Compos Part A: Appl Sci Manuf.* 2010;41(6):759-767. doi:10.1016/j.compositesa.2010.02.008

43. Zhao JB, Wu LL, Zhan CX, Shao Q, Guo ZH, Zhang LQ. Overview of polymer nanocomposites: Computer simulation understanding of physical properties. *Polymer.* 2017;133:272-287. doi:10.1016/j.polymer.2017.10.035

44. Yamamoto N, Hart AJ, Garcia EJ, et al. High-yield growth and morphology control of aligned carbon nanotubes on ceramic fibers for multifunctional enhancement of structural composites. *Carbon.* 2009;47(3):551-560. doi:10.1016/j.carbon.2008.10.030